

Publikacja / Publication	Time-Modulated Antenna Array for real-Time Adaptation in Wideband Wireless Systems-Part I: Design and Characterization, Bogdan Grzegorz, Godziszewski Konrad, Yashchyshyn Yevhen, Kim C.H., Hyun S. B.
DOI wersji wydawcy / Published version DOI	http://dx.doi.org/10.1109/TAP.2019.2902755
Adres publikacji w Repozytorium URL / Publication address in Repository	https://repo.pw.edu.pl/info/article/WUTa78e02c8790f4a71ba538040597be00e/
Data opublikowania w Repozytorium / Deposited in Repository on	Jun 27, 2022
Cytuj tę wersję / Cite this version	Bogdan Grzegorz, Godziszewski Konrad, Yashchyshyn Yevhen, Kim C.H., Hyun S. B.: Time-Modulated Antenna Array for real-Time Adaptation in Wideband Wireless Systems-Part I: Design and Characterization, IEEE Transactions on Antennas and Propagation, vol. 68, no. 10, 2020, pp. 6964- 6972, DOI:10.1109/TAP.2019.2902755

Time-Modulated Antenna Array for Real-Time Adaptation in Wideband Wireless Systems—Part I: Design and Characterization

Grzegorz Bogdan^{ID}, *Student Member, IEEE*, Konrad Godziszewski^{ID}, *Member, IEEE*,

Yevhen Yashchyshyn^{ID}, *Senior Member, IEEE*, Cheol Ho Kim^{ID}, and Seok-Bong Hyun

Abstract—This paper presents a design of a time-modulated antenna array (TMAA) with substantially wider bandwidth and higher efficiency than have already been presented in the literature. The TMAA is designed for 5.4–5.8 GHz frequency band. More than 50 MHz of channel bandwidth is achieved by utilization of ultrafast microwave switches, digital delay lines with 60 ps step, and fast control circuitry. The efficiency is improved by alternate switching between the array elements instead of switching between the array element and a matched load. Moreover, a mathematical derivation of optimal switching sequence is given. The beam steering at the first sideband frequency was obtained with a 1° step in a range from –50° to 50°. The TMAA has been evaluated by means of the radiation pattern measurements at different sideband frequencies.

Index Terms—Adaptive arrays, antenna arrays, antennas, beam steering, radio-frequency (RF) switch, time-modulated antenna array (TMAA), wireless communication.

I. INTRODUCTION

VARIOUS beamforming architectures and algorithms have been invented and implemented to improve the performance of wireless communication and radar systems [1]. Typically, beamforming is achieved by a set of antenna weights (amplitude and/or phase) applied to individual elements [2] in digital domain, analog domain, or both (a hybrid approach). Implementation of digital beamforming is challenging due to constraints of cost, power consumption and signal processing complexity. On the other hand, applicability of the phased antenna array (PAA) is limited by the unsatisfactory performance of phase shifters. Therefore, unconventional array architectures and design methodologies have gained a lot of

Manuscript received August 7, 2018; revised January 23, 2019; accepted February 18, 2019. Date of publication March 4, 2019; date of current version October 6, 2020. This work was supported by ICT R&D Program of Ministry of Science, ICT and Future Planning in South Korea (MSIP)/Institute for Information and Communications Technology Promotion (IITP) [2015-0-00268, Development on semiconductor based smart antenna for future mobile communications]. (Corresponding author: Grzegorz Bogdan.)

G. Bogdan, K. Godziszewski, and Y. Yashchyshyn are with the Institute of Radioelectronics and Multimedia Technology, Warsaw University of Technology, 00-665 Warsaw, Poland (e-mail: g.bogdan@ire.pw.edu.pl; k.godziszewski@ire.pw.edu.pl; y.yashchyshyn@ire.pw.edu.pl).

C. H. Kim and S.-B. Hyun are with the Electronics and Telecommunications Research Institute, Daejeon 34129, South Korea (e-mail: kimcheolho@etri.re.kr; sbhyun@etri.re.kr).

Color versions of one or more of the figures in this article are available online at <http://ieeexplore.ieee.org>.

Digital Object Identifier 10.1109/TAP.2019.2902755

attention over the past two decades [3]. One of the most prospective architectures for a low-cost beamforming is based on time-domain processing [4]. The time-modulated antenna array (TMAA) is an electromagnetic (EM) system whose radiation pattern is controlled by the application of periodical pulses to the individual elements [5]. The TMAA concept is considered as a promising alternative to the PAA because expensive and troublesome phase shifters can be avoided [6]. Output signal of the TMAA is composed of many spectral components (sidebands) at multiples of the modulation frequency around the carrier frequency. This phenomenon used to be considered as a disadvantage. Hence, many techniques for suppression of unwanted sidebands have been proposed [7]–[9]. Alternatively, sidebands can be used to extend capabilities of the TMAA by means of beam steering [4], [10], [11] and spatial diversity [12], [13].

Many practical TMAs employing different switching technologies have been designed and evaluated. Performance of the current state-of-the-art TMAs can be evaluated with the overview of known prototypes presented in Table I. The first figure of merit is the bandwidth that usually does not exceed 5 MHz, which is below the requirements of modern wideband systems. Second crucial parameter is the efficiency. As a matter of fact, TMAs have lower gain than conventional amplitude-tapered arrays when the same patterns are synthesized [14], although exact values of the gain or efficiency are usually not reported. Therefore, the main goal of this paper was to design and evaluate the TMAA with substantially wider bandwidth and higher efficiency than have been already presented in the literature. The TMAA presented in this paper provides an outstanding bandwidth of 50 MHz, which is sufficient to support transmission of wideband signals in most of current wireless systems.

II. SYSTEM FUNDAMENTAL

The proposed TMAA is composed of time-modulated elements (TMEs) distributed with uniform spacing and forming a linear array. TMEs are numbered with $n = 0 \dots N - 1$. Fig. 1 shows a diagram of the TME consisting of two oppositely arranged antennas (such element been already proposed in [28]). If a microwave signal $s_n(t)$ is incident upon the TME

TABLE I
OVERVIEW OF TMAA PROTOTYPES

f_0	f_c	Switch type	Reference
10 kHz	2.45 GHz	SP4T FET	[15]
10 kHz	5 GHz	RPDC p-i-n diode	[16]
10 kHz	9.375 GHz	SPST p-i-n diode	[17]
10 kHz	36 GHz	surface p-i-n diode	[18]
20 kHz	2.4 GHz	SPDT p-i-n diode	[19]
25 kHz	2.45 GHz	Schottky diode	[20]
100 kHz	1.56 GHz	SPST FET	[21]
100 kHz	2.5 GHz	SP3T	[22]
100 kHz	2.45 GHz	Schottky diode	[23]
100 kHz	2.6 GHz	SPST FET	[24]
100 kHz	3.25 GHz	SPST FET	[25]
125 kHz	9.5 GHz	p-i-n diodes	[26]
1 MHz	2.45/5.8 GHz	SPST p-i-n diode	[27]
1 MHz	2.6 GHz	SPDT FET	[28]
1 MHz	2.525 GHz	SPDT CMOS	[29]
1 MHz	2.525 GHz	SP6T	[30]
1.25 MHz	2.6 GHz	SPST FET	[31]
2.5 MHz	5.8 GHz	SP4T p-i-n diode	[32]
5 MHz	2.6 GHz	SPDT FET	[33]
6.49 MHz	5.8 GHz	SPDT p-i-n diode	[34]
50 MHz	5.6 GHz	SPDT	this work

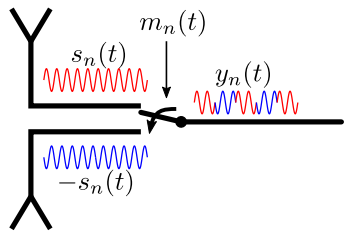


Fig. 1. Diagram of TME.

perpendicularly, then $s_n(t)$ is received by the upper antenna and $-s_n(t)$ is received by the lower antenna (180° phase difference is due to the opposite arrangement of antennas). Next, two signals are delivered to a single-pole double-throw (SPDT) microwave switch that operates alternatively in such a way that the upper antenna is active for duration τ_n , and the lower antenna is active for duration $T_0 - \tau_n$ (the switching is periodical with period T_0). Hence, the output signal $y_n(t)$ is a combination of two signals and has a waveform of a binary phase-keyed signal (similar effect can be achieved by switching between two lines having $\lambda/2$ difference in length [34] or by using two-state phase shifters [35]). Operation of the TME can be expressed as

$$y_n(t) = s_n(t)m_n(t) \quad (1)$$

where $y_n(t)$ is a signal after time modulation, $s_n(t)$ is a single-frequency carrier signal, and $m_n(t)$ is a modulating function. Modulating functions are often assumed to be rectangular or trapezoidal due to the practical reasons [36]. In our case, to represent the operation of the SPDT switch and the opposite arrangement of antennas, $m_n(t)$ has a bipolar rectangular waveform with a high value of 1 and a low value of -1 as illustrated in Fig. 2.

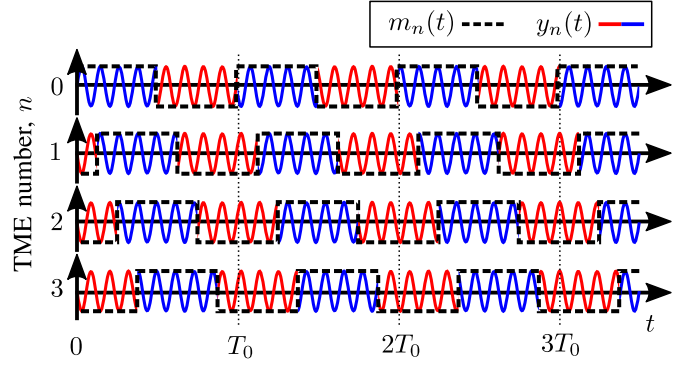


Fig. 2. Modulated signals and progressively delayed modulating functions.

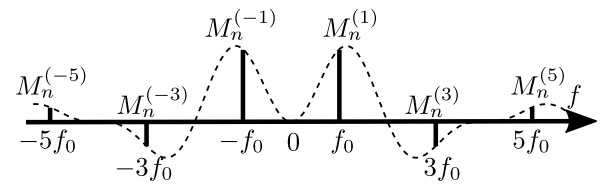


Fig. 3. Spectrum of bipolar modulating function $m_n(t)$ with $\tau_n = T_0/2$ and $\Delta t_n = 0$.

The modulating functions can be expressed as a combination of complex Fourier series coefficients $M_n^{(k)}$ [11]

$$m_n(t) = \sum_{k=-\infty}^{\infty} M_n^{(k)} e^{j2\pi f_0 kt} \quad f_0 = \frac{1}{T_0} \quad (2)$$

$$M_n^{(k)} = \frac{1}{T_0} \int_{-T_0/2}^{T_0/2} m_n(t) e^{-j2\pi f_0 kt} dt \quad (3)$$

where k is the number of the Fourier coefficient. Fig. 3 presents the Fourier coefficients $M_n^{(k)}$ for a special case of $m_n(t)$ with $\tau_n = T_0/2$. There are two advantages when $\tau_n = T_0/2$. First, it maximizes amplitudes of the first negative ($k = -1$) and the first positive ($k = 1$) sideband components. Second, it doubles spacing between sideband components. Both advantages will be explained in Sections II-A and II-C.

The spectrum of the time-modulated signal at the output of each TME can be obtained from

$$Y_n = S_n * M_n \quad (4)$$

where $(*)$ denotes the convolution operator and S_n and M_n are the sets of Fourier series coefficients of the incident signal and the modulating function, respectively.

A. Single-Sideband Efficiency

Time modulation spreads the power of the incident signal to sideband components. Hence, if only one sideband component is used, then the efficiency drops. The shape of the modulating function determines the amplitude and the phase of spectral components. Therefore, appropriate modulating functions should be applied to the array in order to maximize the amplitude of selected sideband component. Fourier series coefficients (3) of bipolar modulating functions, after simple

TABLE II
SINGLE-SIDEBAND EFFICIENCIES

	$\eta_{\text{mod}}^{(0)}$	$\eta_{\text{mod}}^{(-1)}$	$\eta_{\text{mod}}^{(-2)}$	$\eta_{\text{mod}}^{(-3)}$
Without time modulation	100%	0%	0%	0%
SPST with 50% duty cycle	25%	10%	0%	1%
SPDT bipolar (this work)	0%	41%	0%	5%

mathematical operations, can be expressed as

$$M_n^{(k)} = \frac{2\tau_n}{T_0} \text{sinc}\left(k \frac{\tau_n}{T_0}\right) - \text{sinc}(k) \quad (5)$$

where sinc is a normalized sinc function. The highest amplitude for the first negative sideband component ($k = -1$) can be found after taking the derivative of (5) with respect to τ_n

$$\frac{\partial M_n^{(-1)}}{\partial \tau_n} = \frac{2}{T_0} \cos\left(\frac{\pi \tau_n}{T_0}\right) = 0 \Rightarrow \tau_n = \frac{T_0}{2}. \quad (6)$$

Thus, the highest single-sideband efficiency, $\eta_{\text{mod}}^{(k)}$, is obtained for equal switching between two antennas of the TME. The single-sideband efficiency can be calculated as the power ratio of the selected sideband component to the total power of the signal, i.e., if $k = -1$, then

$$\eta_{\text{mod}}^{(-1)} = \frac{|Y_n^{(-1)}|^2}{\sum_{k=-\infty}^{\infty} |Y_n^{(k)}|^2} = \frac{|M_n^{(-1)}|^2}{\sum_{k=-\infty}^{\infty} |M_n^{(k)}|^2} = 41\%. \quad (7)$$

Single-sideband efficiency of the proposed TMAA is four times higher than the efficiency obtained with absorptive single-pole single-throw (SPST) switches with 50% duty cycle. Comparison of single-sideband efficiencies for different methods of time modulation is presented in Table II.

B. Radiation Efficiency

The radiation efficiency (η_{rad}) is defined as the ratio of the total power radiated by an antenna to the net power accepted by the antenna from the connected transmitter [37]. Typically, for a conventional antenna (without time modulation), the radiation efficiency is used to take into account the losses at the input terminals and within the structure of the antenna. This includes conduction and dielectric losses (η_{cd}) and losses due to the reflections because of the mismatch between the transmission line and the antenna $\eta_r = 1 - |\Gamma|^2$, where Γ is the voltage reflection coefficient at the input terminals of the antenna [2]. In the case of the TMAA, the following three additional factors should be considered.

- 1) The reflection losses caused by the impedance mismatch between transmission lines and ports of the radio frequency (RF) switch.
- 2) The efficiency of RF switches which can be defined as $\eta_{\text{sw}} = 1/L_{\text{sw}}$, where (L_{sw} is the insertion loss given in linear scale).
- 3) The efficiency drop caused by absorptive switches when turned off (η_{OFF}).

After consideration of all the aforementioned factors, the radiation efficiency of the TMAA can be written as

$$\eta_{\text{rad}} = \eta_r \eta_{\text{cd}} \eta_{\text{sw}} \eta_{\text{OFF}} \quad (8)$$

The efficiency calculations for the designed antenna are presented in Section IV-C.

C. Maximum Signal Bandwidth

Typically, the modulation frequency should be greater than the bandwidth of a linearly modulated digital signal to avoid overlapping of the spectral replicas [38]. However, the TMAA proposed in this paper can be used to transmit signals exceeding this limitation. This is possible because the center frequency component and the evenly numbered sideband components are not present.

The center frequency component ($k = 0$) is not present because the 180° phase shift due to the opposite arrangement of patches is not compensated with a phase shift due to the time modulation. This phenomenon occurs only if an incident wave is perpendicular to the TME. Otherwise, the center frequency component will not be completely canceled but suppressed dependently on the incident angle.

Spectral components of even orders are not present because the sinc function has nulls in these points

$$M_n^{(k)} = \text{sinc}\left(\frac{k}{2}\right) - \text{sinc}(k) = 0 \quad \text{if } k = 0, \pm 2, \pm 4, \dots \quad (9)$$

Therefore, only odd sideband components ($k = \pm 1, \pm 3, \pm 5, \dots$) exist, which doubles the bandwidth.

D. Beam Steering

Let us now consider a TMAA composed of $N = 4$ linearly and uniformly distributed TMEs, where modulating functions are bipolar square waveforms with $\tau_n = T_0/2$, $\forall n = 0 \dots N - 1$ and are delayed by Δt_n with respect to the first modulating function $m_0(t)$ ($\Delta t_0 = 0$). Fig. 2 presents an example of such modulating functions. Output $f(t)$ from the array is a superposition of the time-modulated signals $y_n(t)$ from all TMEs

$$f(t) = \sum_{n=0}^{N-1} y_n(t) = \sum_{n=0}^{N-1} s_n(t)m_n(t) \xrightarrow{\mathcal{F}} F = \sum_{n=0}^{N-1} S_n * M_n. \quad (10)$$

Phase control can be applied to the modulating functions on the basis of a well-known time-shift property of the Fourier series, which states that the time delay Δt_n in the time domain causes the phase shift in the frequency domain

$$m_n(t) = m_0(t - \Delta t_n) \Rightarrow M_n^{(k)} = M_0^{(k)} e^{-j2\pi k \Delta t_n / T_0} \quad (11)$$

Therefore, delays of modulating functions, Δt_n , cause the phase shift similar to a conventional phased array. For example, if $T_0 = 20$ ns and $\Delta t_n = 0.056$ ns, then -1° phase shift on the first negative sideband component is achieved. Beam steering can be achieved by the phase progression on the sideband components due to delay progression of modulating functions $\Delta t = \Delta t_{n+1} - \Delta t_n$, i.e., the delay of modulating functions for consecutive TMEs is increased by Δt with respect to the preceding TME

$$m_n(t) = m_0(t - n\Delta t). \quad (12)$$

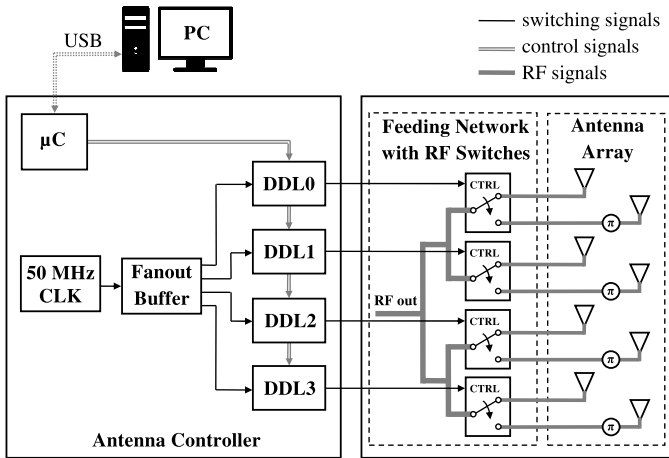


Fig. 4. Schematic of TMAA.

Hence, the first negative sideband component of the output signal of the beam-steering TMAA can be expressed as

$$\begin{aligned} F^{(-1)} &= M_0^{(-1)} \sum_{n=0}^{N-1} S_n e^{j2\pi \Delta t_n / T_0} \\ &= M_0^{(-1)} \sum_{n=0}^{N-1} S_n e^{j2\pi n \Delta t / T_0}. \end{aligned} \quad (13)$$

III. PROPOSED TMAA SYSTEM

The TMAA forms a system that includes an antenna array with switches, an antenna controller, and an adaptive algorithm. Schematic of the system is presented in Fig. 4. The design, principles of operation, and microwave measurements are described in this section. Adaptive algorithm and the study of adaptation are presented in the second part of this paper [39].

A. Antenna Array With RF Switches

The TME shown in Fig. 1 was implemented as a structure composed of two oppositely oriented aperture-coupled series-fed patches. This TMAA design has been already proposed [28]. However, it is now improved with a second patch to increase the gain and to narrow the main beam in the E-plane (yz plane). Patch antennas are formed on a superstrate above the ground plane and are electromagnetically coupled with the feeding network through small apertures (slots in the ground plane). The aperture-coupled design is particularly advantageous when applied to TMAs because the ground plane shields the antenna from spurious radiation emitted by feedlines and microwave switches. Moreover, with the two-layer design, patches are located on a lower permittivity substrate ($\epsilon_r = 2.2$), which provides wide impedance bandwidth and high radiation efficiency, whereas the feeding network lays on a higher permittivity substrate ($\epsilon_r = 3.66$) that yields lower radiation losses [40].

Four TMEs were used to form an antenna array with beam-steering capability in the H-plane (xz plane). The

TABLE III
COMPARISON OF SPDT SWITCHES

Ref	L_{sw} (dB)	$ \Gamma $ (dB)	t_{RF}^{sw} (ns)	B (GHz)	P_{max} (dBm)	Technology
[43]	0.5	-20	20	DC-20	33	Si p-i-n
[44]	2.0	-10	3	DC-8	27	GaAs MESFET
[45]	1.7	-17	2	DC-20	30	GaAs pHEMT
[41]	1.2	-22	2	DC-30	27	Si
[42]	1.3	-5	0.03	42-70	1	SiGe HBT

antenna was fabricated in a multilayer printed circuit board technology. The top layer with patch antennas is presented in Fig. 5(a) and the bottom layer with switches is presented in Fig. 5(b). Fig. 5(a) shows also the radiation pattern of a 30° beam simulated in an EM computer software.

RF switches are critical elements of the time modulation circuitry. The RF rise/fall time of the switch determines the maximum bandwidth of a signal that can be transmitted/received by the TMAA without overlapping of spectral replicas. In order to achieve wideband operation, very short switching time $t_{RF}^{sw} < 5$ ns from 10% to 90% RF is necessary. In addition to timing parameters, microwave parameters have to be considered as well, i.e., insertion loss (L_{sw}) and reflection loss ($|\Gamma|$). Comparison of high-performance switches is presented in Table III. Switch ADRF5020 [41] was selected based on ultrashort switching time ($t_{RF}^{sw} = 2$ ns) and very good microwave performance at 5.6 GHz. It is worth mentioning that ultrafast switches with $t_{RF}^{sw} < 0.1$ ns operating in mm-wave have been already presented in the literature [42] and hopefully will be available commercially for further improvement of the TMAA performance.

B. Antenna Controller

The antenna controller changes the states of RF switches in the required timing. It should provide a high pulse repetition frequency and a variable delay of control signals. The controller proposed in this paper is similar to the one presented in [34], although, in our case, much higher modulation frequency was obtained. Its schematic and photograph after fabrication are presented in Figs. 4 and 5(c), respectively. The design is straightforward, thanks to the low-voltage transistor-transistor logic (LVTTL)/CMOS driver built inside the RF switch [41]. Moreover, due to the 50% duty cycle of all modulating functions, a commercial 50 MHz microelectromechanical system (MEMS) clock signal generator with high stability of ± 10 ppm could be used (the controller has been also tested with higher frequencies of the clock signal generator, i.e., 80, 100, and 125 MHz). Delays are applied with 8-bit programmable digital delay lines (DDLs) with a fine step of 60 ps and a maximum value of 15.3 ns [46]. Fig. 6 and Table IV give examples of DDL settings directing the beam for $k = -1$ toward angle θ_{max}^{-1} . For example, if $\theta_{max}^{-1} = -45^\circ$ is required, then $\Delta t = -0.441T_0$. Thus, for $T_0 = 50$ MHz, $\Delta t_0 = 0$ ns, $\Delta t_1 = -8.82$ ns, $\Delta t_2 = -17.64$ ns, and $\Delta t_3 = -26.46$ ns. Next, due to the periodicity of modulating functions, we can add 20 ns to both the second and the third delays, hence $\Delta t_2 = 2.36$ ns and $\Delta t_3 = -6.46$ ns.

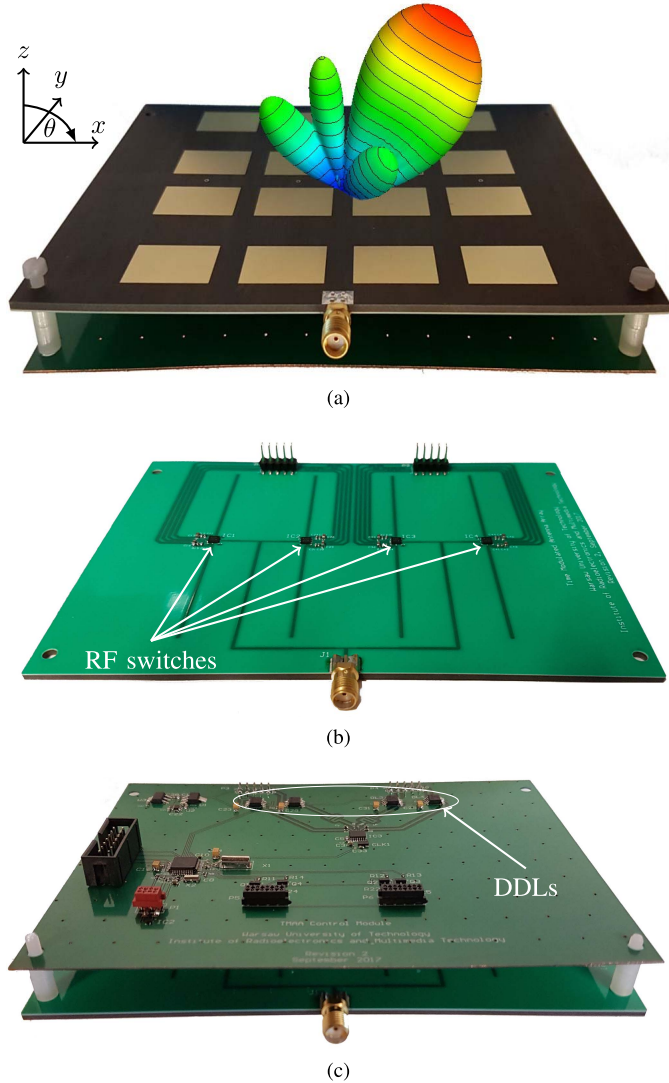


Fig. 5. Fabricated TMAA. (a) Top layer with patch antennas and simulated 3-D pattern of 30° beam. (b) Bottom layer with feeding network and switches. (c) Control board.

Negative delays are not possible to apply, and therefore, a constant value of 8.82 ns is added to all delays in order to obtain the positive values without losing the relative relations: $\Delta t_0 = 8.82$ ns, $\Delta t_1 = 0$ ns, $\Delta t_2 = 11.18$ ns, and $\Delta t_3 = 2.36$ ns. Then, the values are divided by the step of 60 ps to obtain register values: $DDL0 = 147$, $DDL1 = 0$, $DDL2 = 187$, and $DDL3 = 40$.

Each DLL is programmed by a personal computer (PC) via a universal serial bus, which is used also as a power supply for all active components. A microcontroller is used to receive data from the PC and to set delays on four daisy-chained DLLs.

IV. CHARACTERIZATION OF DESIGNED TMAA

A. Switching

Parameters of the selected switch were measured on a test board with a sampling oscilloscope. The measured output signal is presented in Fig. 7. The RF rise time from 10% to 90% of the maximum amplitude is around 1.5 ns. The duty

TABLE IV
SETTINGS OF DDLs

DDL0	DDL1	DDL2	DDL3	$\Delta t/T_0$	Δt (ns)	θ_{\max}^{-1}
147	0	187	40	-0.441	-8.82	-45°
198	132	66	0	-0.198	-3.96	-20°
0	0	0	0	0	0	0°
0	66	132	198	0.198	3.96	20°
40	187	0	147	0.441	8.82	45°

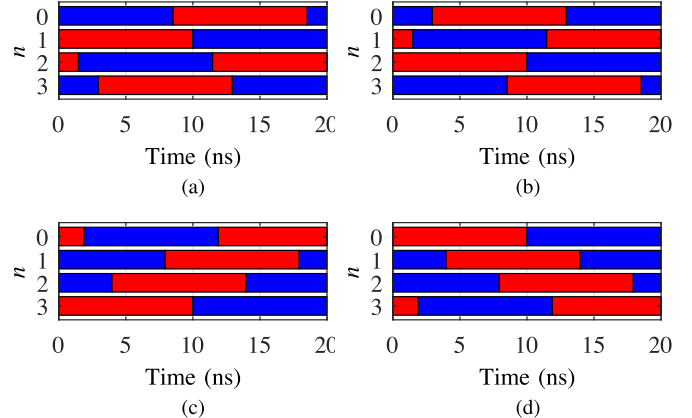


Fig. 6. Examples of switching sequences (blue and red colors represent switching between two antennas in TME).

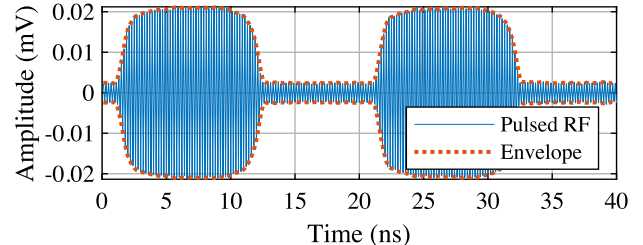


Fig. 7. Output of RF switch.

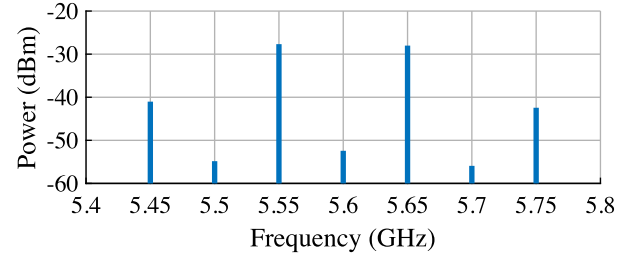


Fig. 8. Measured spectrum of TMAA output signal.

cycle measured between 50% of the rising edge and 50% of the falling edge is close to a half of the modulation period $T_0/2 = 10$ ns.

B. Bandwidth

Fig. 8 shows the measured spectrum of a signal at the output of the TMAA when illuminated from broadside direction $\theta = 0^\circ$ with a continuous-wave signal with $f_c = 5.6$ GHz (without progressive delay, i.e., $\Delta t = 0$). The settings of

TABLE V
SETTINGS OF SPECTRUM ANALYZER

Parameter	Setting
Center frequency	5.6 GHz
Frequency span	500 MHz
Number of points	101
Resolution bandwidth	1 MHz
Detector type	Sampling detector

the measurement are gathered in Table V. The levels of the center frequency component and evenly ordered components are, respectively, 25 and 27 dB lower than the level of the first sideband component. Therefore, if $f_0 = 50$ MHz, it is possible in some conditions to transmit a signal with a maximum bandwidth of 100 MHz because the degradation of the SNR due to overlapping of spectral replicas will be negligible.

C. Efficiency and Gain

The radiation efficiency, (η_r), of designed TMAA can be calculated according to (8), after consideration of following partial efficiencies.

- 1) $\eta_{\text{OFF}} = 1$, because the proposed architecture does not dissipate the power in OFF-state.
- 2) $\eta_r \approx 1$, thanks to negligibly low impedance mismatch between microstrip lines, patch antennas, and switches.
- 3) $\eta_{\text{ed}} = 0.8$, due to the efficient design of the antenna array (the value was computed using an EM simulator).
- 4) $\eta_{\text{sw}} = 1/1.32 = 0.76$, because the insertion loss of the RF switch $L_{\text{sw}} = 1.2$ dB (1.32 in linear scale).

Hence, $\eta_{\text{rad}} = 0.6$. The TMAA system efficiency, which includes all RF losses and efficiency of the first negative sideband component, equals

$$\eta_{\text{TMAA}}^{(-1)} = \eta_{\text{rad}} \eta_{\text{mod}}^{(-1)} = 0.6 \cdot 0.41 \approx 0.25 \quad (14)$$

In order to calculate the TMAA gain, both the directivity and the efficiency should be considered. The directivity $D = 16.5$ dBi was obtained from EM simulations. However, the simulations were performed for a static excitation of all array elements. In case of the proposed TMAA, only half of the elements are active, and therefore, the aperture efficiency $\eta_a = 0.5$. Eventually, the calculated TMAA gain at the first negative sideband component equals

$$G_{\text{TMAA}}^{(-1)} = D \eta_{\text{TMAA}}^{(-1)} \eta_a = 7.4 \text{ dBi.} \quad (15)$$

The calculations were confirmed by means of measurements for $k = \{-1, 0, +1\}$ and variable carrier frequency f_c . The obtained values of the TMAA gain are presented in Fig. 9.

D. Radiation Patterns and Beam Steering

Radiation patterns of antennas are typically obtained from the measurements of the transmission coefficient acquired with the vector network analyzer. However, in the case of the TMAA, the transmitting and the receiving frequencies may differ. In consequence, it is not possible to directly measure the TMAA pattern [47], and therefore, a procedure based on a microwave signal generator and a spectrum analyzer was

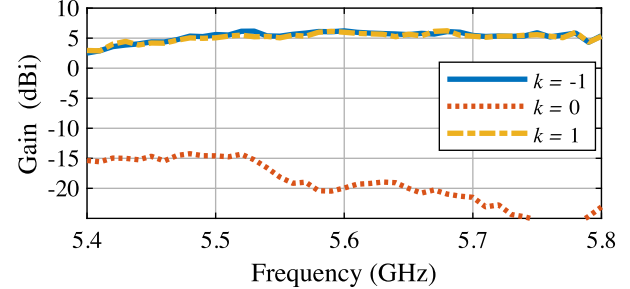


Fig. 9. Measured gain of TMAA.

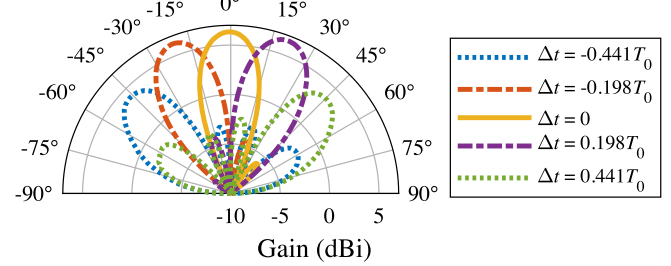


Fig. 10. Radiation patterns in H-plane measured at $k = -1$ for different Δt .

used [48]. A total number of 121 beams steered from -60° to 60° with 1° step were measured. The selected radiation patterns measured in the H-plane at $k = -1$ for delays gathered in Table IV are presented in Fig. 10. The highest TMAA gain $G_{\text{TMAA}}^{(-1)} = 7$ dBi was measured for 0° beam. In this case, the half-power beamwidth HPBW = 24° and the sidelobe level SSL = 14 dB. The gain drops when increasing the scanning angle, reaching $G_{\text{TMAA}}^{(-1)} = 3.5$ dBi for 50° beam. For wider scanning angles, the sidelobe level increases. Therefore, satisfactory scanning sector is 100° wide. The set of measured beams was used to implement an adaptive antenna system, which is described in the second part of this paper [39].

The radiation patterns measured at sideband components $k = \{1, 3, 5\}$ without steering ($\Delta t = 0$) are presented in Fig. 11. The radiation patterns have almost identical shape and, however, different gains. The gain drops more than 10 dB for $k = 3$ and more than 25 dB for $k = 5$, which corresponds with measurements of spectrum (Fig. 8). Fig. 12 shows the radiation patterns measured at the same sideband frequencies as presented in Fig. 11, although with $\Delta t = 0.1T_0$. The radiation patterns measured at the sideband components of higher orders are steered toward larger angles proportionally to its order. Such diversity of beams can be used for multichannel spatial transmission.

Radiation patterns measured for various frequencies of time modulation $f_0 \in \{50, 80, 100, 125\}$ MHz are presented in Fig. 13. If the time-modulation frequency increases, then the duration of transient between two states of the RF switch become more significant in relation to the modulation period. The highest gain was achieved for $f_0 = 50$ MHz. Faster control of the RF switch leads to a decrease of the gain. On the other hand, higher f_0 enables transmission of signals with a

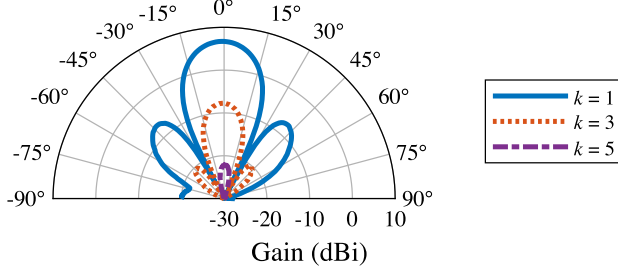
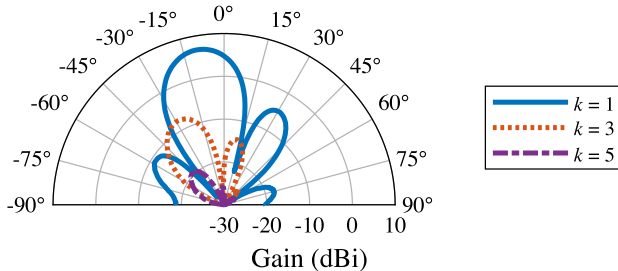
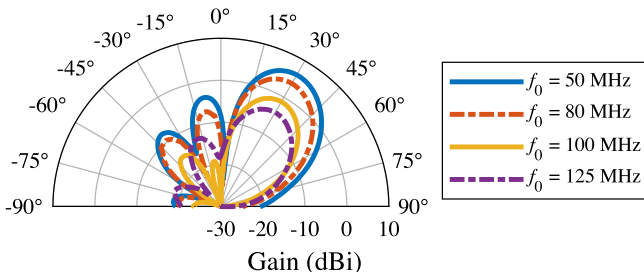
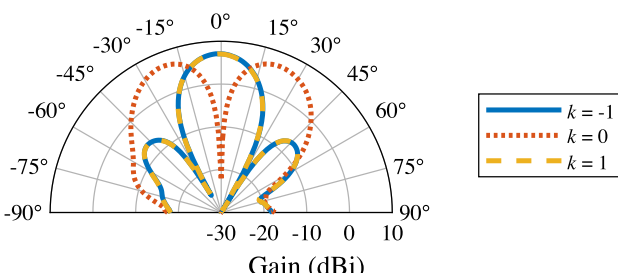
Fig. 11. Measured radiation patterns in H-plane for $\Delta t = 0$.Fig. 12. Measured radiation patterns in H-plane for $\Delta t = 0.1T_0$.Fig. 13. Radiation patterns of 15° beam measured for various modulation frequencies.

Fig. 14. Radiation patterns in E-plane.

wider bandwidth. Therefore, a satisfactory tradeoff between the gain and the system bandwidth should be found when applying the TMAA into a wireless system.

According to the spectral analysis presented in Fig. 8, the radiation pattern at the center frequency ($k = 0$) has a deep null in a broadside direction. This was confirmed by the radiation pattern measurements in the E-plane (nonscanning plane) presented in Fig. 14. The gain at the center frequency is less than 0 dBi for the angular sector of 10° . Therefore, the center component may limit the maximum bandwidth of

signals if they are arriving from diverse directions, especially in multipath environments.

V. CONCLUSION

Improvement of the TMAA efficiency was achieved by means of alternative switching between a pair of elements connected to an SPDT switch. In addition, the proposed method of time modulation avoided generation of evenly numbered sideband components, which led to a wider bandwidth.

An outstanding bandwidth of 50 MHz was achieved as a result of a very short switching time of the state-of-the-art RF switches applied in the presented design of the TMAA. In addition, a specially designed controller based on a MEMS clock signal generator and programmable semiconductor delay lines with a 60 ps delay step was used to perform beam steering with a 1° resolution. Good efficiency, wide bandwidth, and beam-steering capability of the TMAA prove its high potential as an adaptive antenna for wireless communication devices.

REFERENCES

- [1] R. A. Monzingo, R. L. Haupt, and T. W. Miller, *Introduction to Adaptive Arrays*. Rijeka, Croatia: SciTech, 2011.
- [2] C. A. Balanis, *Antenna Theory: Analysis and Design*. Hoboken, NJ, USA: Wiley, 2012.
- [3] P. Rocca, G. Oliveri, R. J. Mailloux, and A. Massa, "Unconventional phased array architectures and design methodologies—A review," *Proc. IEEE*, vol. 104, no. 3, pp. 544–560, Mar. 2016.
- [4] H. Shanks, "A new technique for electronic scanning," *IRE Trans. Antennas Propag.*, vol. 9, no. 2, pp. 162–166, Mar. 1961.
- [5] R. Maneiro-Catona, J. Brégains, J. A. García-Naya, and L. Castedo, "Time modulated arrays: From their origin to their utilization in wireless communication systems," *Sensors*, vol. 17, no. 3, p. 590, Mar. 2017.
- [6] Y. Yashchyshyn, K. Godziszewski, G. Bogdan, and P. Piasecki, "X-band antenna array for low-cost beam scanning," *IET Microw. Antennas Propag.*, vol. 11, no. 15, pp. 2174–2178, Dec. 2017.
- [7] S. Yang, Y. B. Gan, and A. Qing, "Sideband suppression in time-modulated linear arrays by the differential evolution algorithm," *IEEE Antennas Wireless Propag. Lett.*, vol. 1, no. 1, pp. 173–175, Feb. 2002.
- [8] D. Gwak, I. Sohn, and S. H. Lee, "Analysis of single-RF MIMO receiver with beam-switching antenna," *ETRI J.*, vol. 37, no. 4, pp. 647–656, Aug. 2015.
- [9] T. D. Drysdale, B. Allen, and E. Okon, "Sinusoidal time-modulated uniform circular array for generating orbital angular momentum modes," in *Proc. 11th Eur. Conf. Antennas Propag. (EUCAP)*, Paris, France, Mar. 2017, pp. 973–977.
- [10] C. He, L. Wang, J. Chen, and R. Jin, "Time-modulated arrays: A four-dimensional antenna array controlled by switches," *J. Commun. Inf. Netw.*, vol. 3, no. 1, pp. 1–14, Mar. 2018.
- [11] L. Poli, P. Rocca, G. Oliveri, and A. Massa, "Harmonic beamforming in time-modulated linear arrays," *IEEE Trans. Antennas Propag.*, vol. 59, no. 7, pp. 2538–2545, Jul. 2011.
- [12] P. Rocca, Q. Zhu, E. T. Bekele, S. Yang, and A. Massa, "4-D arrays as enabling technology for cognitive radio systems," *IEEE Trans. Antennas Propag.*, vol. 62, no. 3, pp. 1102–1116, Mar. 2014.
- [13] R. Maneiro-Catona and J. C. Brégains, J. A. García-Naya, L. Castedo, P. Rocca, and L. Poli, "Performance analysis of time-modulated arrays for the angle diversity reception of digital linear modulated signals," *IEEE J. Sel. Topics Signal Process.*, vol. 11, no. 2, pp. 247–258, Mar. 2017.
- [14] Q. Zhu, S. Yang, R. Yao, and Z. Nie, "Gain improvement in time-modulated linear arrays using SPDT switches," *IEEE Antennas Wireless Propag. Lett.*, vol. 11, pp. 994–997, 2012.
- [15] G. Bogdan, P. R. Bajurko, and Y. Yashchyshyn, "Null-steering in two-element time modulated linear antenna array through pulse-delay approach," in *Proc. 20th Int. Conf. Microw., Radar Wireless Commun. (MIKON)*, Gdańsk, Poland, Jun. 2014, pp. 1–4.

- [16] J. Chen *et al.*, "Efficiency improvement of time modulated array with reconfigurable power divider/combiner," *IEEE Trans. Antennas Propag.*, vol. 65, no. 8, pp. 4027–4037, Aug. 2017.
- [17] W. H. Kummer, A. T. Villeneuve, T. Fong, and F. Terrio, "Ultra-low sidelobes from time-modulated arrays," *IEEE Trans. Antennas Propag.*, vol. AP-11, no. 6, pp. 633–639, Nov. 1963.
- [18] Y. Yashchyshyn, K. Derzakowski, P. R. Bajurko, J. Marczewski, and S. Kozłowski, "Time-modulated reconfigurable antenna based on integrated S-PIN diodes for mm-Wave communication systems," *IEEE Trans. Antennas Propag.*, vol. 63, no. 9, pp. 4121–4131, Sep. 2015.
- [19] A. Tennant, "Experimental two-element time-modulated direction finding array," *IEEE Trans. Antennas Propag.*, vol. 58, no. 3, pp. 986–988, Mar. 2010.
- [20] D. Masotti, A. Costanzo, M. Del Prete, and V. Rizzoli, "Time-modulation of linear arrays for real-time reconfigurable wireless power transmission," *IEEE Trans. Microw. Theory Techn.*, vol. 64, no. 2, pp. 331–342, Jan. 2016.
- [21] S. Yang, Y. B. Gan, A. Qing, and P. K. Tan, "Design of a uniform amplitude time modulated linear array with optimized time sequences," *IEEE Trans. Antennas Propag.*, vol. 53, no. 7, pp. 2337–2339, Jul. 2005.
- [22] A.-M. Yao, W. Wu, and D.-G. Fang, "Study on reconfigurable coaperture antenna arrays based on time-modulation and retrodirective techniques," *IEEE Trans. Antennas Propag.*, vol. 64, no. 5, pp. 1713–1724, May 2016.
- [23] P. Rocca, D. Masotti, A. Costanzo, M. Salucci, and L. Poli, "The role of accurate dynamic analysis for evaluating time-modulated arrays performance," *IEEE Antennas Wireless Propag. Lett.*, vol. 16, pp. 2663–2666, 2017.
- [24] Q. Zhu, S. Yang, R. Yao, M. Huang, and Z. Nie, "Unified time- and frequency-domain study on time-modulated arrays," *IEEE Trans. Antennas Propag.*, vol. 61, no. 6, pp. 3069–3076, Jun. 2013.
- [25] Q. Zhu, S. Yang, L. Zheng, and Z. Nie, "Design of a low sidelobe time modulated linear array with uniform amplitude and sub-sectional optimized time steps," *IEEE Trans. Antennas Propag.*, vol. 60, no. 9, pp. 4436–4439, Sep. 2012.
- [26] Y. Wang and A. Tennant, "Experimental time-modulated reflector array," *IEEE Trans. Antennas Propag.*, vol. 62, no. 12, pp. 6533–6536, Dec. 2014.
- [27] R. Gahley and B. Basu, "A time modulated printed dipole antenna array for beam steering application," *Int. J. Antennas Propag.*, vol. 2017, Feb. 2017, Art. no. 3687293.
- [28] G. Bogdan, Y. Yashchyshyn, and M. Jarzynka, "Time-modulated antenna array with lossless switching network," *IEEE Antennas Wireless Propag. Lett.*, vol. 15, pp. 1827–1830, 2016.
- [29] C. He, X. Liang, Z. Li, J. Geng, and R. Jin, "Direction finding by time-modulated array with harmonic characteristic analysis," *IEEE Antennas Wireless Propag. Lett.*, vol. 14, pp. 642–645, Nov. 2014.
- [30] C. He, X. Liang, B. Zhou, J. Geng, and R. Jin, "Space-division multiple access based on time-modulated array," *IEEE Antennas Wireless Propag. Lett.*, vol. 14, pp. 610–613, Nov. 2014.
- [31] C. He *et al.*, "Direction finding by time-modulated linear array," in *Proc. IEEE Int. Symp. Antennas Propag. USNC/URSI Nat. Radio Sci. Meeting*, San Diego, CA, USA, Jul. 2017, pp. 315–316.
- [32] J. D. Fredrick, Y. Wang, and T. Itoh, "A smart antenna receiver array using a single RF channel and digital beamforming," *IEEE Trans. Microw. Theory Techn.*, vol. 50, no. 12, pp. 3052–3058, Dec. 2002.
- [33] G. Jo, J.-N. Lee, H.-O. Bae, Y.-H. Lee, D. Gwak, and J.-H. Oh, "LTE based spatial multiplexing MIMO with single radio," in *Proc. 46th Eur. Microw. Conf. (EuMC)*, London, U.K., Oct. 2016, pp. 1319–1322.
- [34] S. Farzaneh and A.-R. Sebak, "Microwave sampling beamformer-prototype verification and switch design," *IEEE Trans. Microw. Theory Techn.*, vol. 57, no. 1, pp. 36–44, Jan. 2009.
- [35] A. M. Yao, W. Wu, and D. G. Fang, "Single-sideband time-modulated phased array," *IEEE Trans. Antennas Propag.*, vol. 63, no. 5, pp. 1957–1968, May 2015.
- [36] E. T. Bekele, L. Poli, P. Rocca, and M. D'Urso, and A. Massa, "Pulse-shaping strategy for time modulated arrays—Analysis and design," *IEEE Trans. Antennas Propag.*, vol. 61, no. 7, pp. 3525–3537, Jul. 2013.
- [37] *Standard for Definitions of Terms for Antennas*, IEEE Standard 145-1993, 2014.
- [38] R. Maneiro-Catoira, J. C. Brégains, J. A. Garvía-Naya, and L. Castedo, "On the feasibility of time-modulated arrays for digital linear modulations: A theoretical analysis," *IEEE Trans. Antennas Propag.*, vol. 62, no. 12, pp. 6114–6122, Dec. 2014.
- [39] G. Bogdan, K. Godziszewski, and Y. Yashchyshyn, "Time modulated antenna array for real-time adaptive beamforming in wideband wireless systems—Part II: Adaptation study," *IEEE Trans. Antennas Propag.*, vol. 68, no. 10, pp. 6973–6982, Oct. 2020.
- [40] P. Sullivan and D. H. Schaubert, "Analysis of an aperture coupled microstrip antenna," *IEEE Trans. Antennas Propag.*, vol. AP-34, no. 8, pp. 977–984, Aug. 1986.
- [41] Analog Devices. (Dec. 2017). *ADRF5020—100 MHz to 30 GHz, Silicon SPDT Switch*. [Online]. Available: <http://www.analog.com/media/en/technical-documentation/data-sheets/ADRF5020.pdf>
- [42] M. Thian and V. F. Fusco, "Ultrafast low-loss 42–70 GHz differential SPDT switch in 0.35 μm SiGe technology," *IEEE Trans. Microw. Theory Techn.*, vol. 60, no. 3, pp. 655–659, Mar. 2012.
- [43] MACOM. (Jan. 2018). *MASW-00x100 Series HMIC Silicon PIN Diode Switches*. [Online]. Available: <https://cdn.macom.com/datasheets/MASW-00x100.pdf>
- [44] Analog Devices. (Jun. 2018). *HMC347C8—GaAs MMIC SMT High Isolation SPDT Switch, DC—8 GHz*. [Online]. Available: <http://www.analog.com/media/en/technical-documentation/datasheets/hmc347c8.pdf>
- [45] Analog Devices. (2018). *HMC547ALP3E—GaAs MMIC SPDT Non-Reflective Switch, DC—20 GHz*. [Online]. Available: <http://www.analog.com/media/en/technical-documentation/datasheets/HMC547ALP3E.pdf>
- [46] Data Delay Devices. (Dec. 2017). *Monolithic 8-Bit Programmable Delay Line (Series 3D3438)*. [Online]. Available: <http://www.datadelay.com/datasheets/3d3438.pdf>
- [47] S. Farzaneh, A. K. Ozturk, A. R. Sebak, and R. Paknys, "Antenna-pattern measurement using spectrum analyzer for systems with frequency translation," *IEEE Antennas Propag. Mag.*, vol. 51, no. 3, pp. 126–131, Jun. 2009.
- [48] G. Bogdan, K. Godziszewski, and Y. Yashchyshyn, "Feasibility of standard instrumentation for radiation pattern measurement of time modulated antenna array," in *Proc. 22nd Int. Microw. Radar Conf. (MIKON)*, Poznań, Poland, Jun. 2018, pp. 420–423.



Grzegorz Bogdan (S'16) was born in Poland in 1989. He received the B.E. and M.E. degrees in electrical and computer engineering from the Warsaw University of Technology (WUT), Warsaw, Poland, in 2012 and 2013, respectively, where he is currently pursuing the Ph.D. degree.

In 2013, he was an Exchange Student with the University of Waterloo. Since 2016, he has been with the Institute of Radioelectronics and Multimedia Technology, WUT, where he is currently an Assistant. His current research interests include reconfigurable antenna arrays, time modulation, and wireless communications.



Konrad Godziszewski (S'12–M'17) was born in Warsaw, Poland, in 1986. He received the M.E. degree in electronics and telecommunications and Ph.D. degree in telecommunications from the Warsaw University of Technology (WUT), Warsaw, Poland, in 2011 and 2018, respectively.

In 2013, he joined the Institute of Radioelectronics and Multimedia Technology, WUT, where he is currently an Assistant Professor. He has authored or co-authored more than 50 technical papers. His current research interests include antennas, material characterization in subterahertz frequency range, and ferroelectric materials.



Yevhen Yashchyshyn (M'96–SM'09) received the M.E. degree from Lviv Polytechnic National University, Lviv, Ukraine, in 1979, the Ph.D. degree from the Moscow Institute of Electronics and Mathematics, Moscow, Russia, in 1986, and the D.Sc. (Habilitation) degree from the Warsaw University of Technology (WUT), Warsaw, Poland, in 2006.

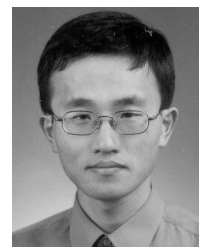
In 2016, he was promoted to a Professor. Since 1999, he has been with the Institute of Radioelectronics and Multimedia Technology, WUT, where he is currently a Professor and the Deputy Director for Research. He has authored more than 250 technical papers and has authored or co-authored 5 books. He holds several patents. His current research interests include antenna theory and techniques, smart beamforming, reconfigurable antennas, radio-over-fiber techniques, and materials characterization, including ferroelectric ceramic-polymers composites investigation up to subterahertz frequency.

Prof. Yashchyshyn was a recipient of the First Prize of EuMA at the 11th European Microwave Week for his outstanding research and new concept of the reconfigurable antenna, Amsterdam, The Netherlands, in 2008.



Cheol Ho Kim received the B.S., M.S., and Ph.D. degrees in electrical engineering from Korea Institute of Science and Technology, Daejeon, South Korea, in 2004, 2006, and 2012, respectively.

He is currently a Senior Research Engineer with the Electronics and Telecommunication Research Institute, Daejeon. He is currently involved with development of new machine learning algorithms for cognitive artificial intelligence (AI). His current research interests include wireless communication systems, monolithic microwave integrated circuits, power amplifiers, machine learning, and AI.



Seok-Bong Hyun received the B.S., M.S., and Ph.D. degrees in applied physics from the Korea Advanced Institute of Science and Technology, Daejeon, South Korea, in 1991, 1993, and 1998, respectively.

In 1999, he joined the Electronics and Telecommunications Research Institute, Daejeon, where he has been involved in the design of RF and analog integrated circuits for short-range wireless communication systems and semiconductor-based beamforming antenna. His current research interests include the design of mixed signal IC and millimeter wave

radio for 5G and beyond network.